CHEMICAL ENGINEERING TRANSACTIONS
VOL. 105, 2023
A publication of AIDIC
The Italian Association of Chemical Engineering
Online at www.cetjournal.it
Guest Editors: David Bogle, Flavio Manenti, Piero Salatino

ISBN 979-12-81206-04-5; **ISSN** 2283-9216
DOI: 10.3303/CET23105054

Kinetics of Catalytic Oxidation of Hydroxymethylfurfural to 2,5-Furandicarboxylic Acid over $LaMn_{1-x}Ni_xO_{3-d}$ Perovskite Oxide

Piyachat Wattanachai[a], Soipatta Soisuwan[a,b], Patiparn Boonruam[a,b], Joongjai Panpranot[c], Pinit Kidkhunthod[d], Settakorn Upasen[a,b]

[a]Department of Chemical Engineering, Engineering Faculty, Burapha University, Chonburi, Thailand
[b]Research Unit of Developing Technology and Innovation of Alternative Energy for Industries, Burapha University, Chonburi, Thailand
[c]Center of Excellence on Catalysis and Catalytic Reaction Engineering, Department of Chemical Engineering, Faculty of Engineering, Chulalongkorn University, Bangkok, 10330, Thailand
[d]Synchrotron Light Research Institute (Public Organization), Nakhon Ratchasima, 30000, Thailand
settakorn@eng.buu.ac.th

This present research aims at studying the kinetic reaction of HMF oxidation which is influenced by temperature gradient and Mn/Ni cation ratio in a lanthanum-based perovskite oxide catalyst. The result can be a fruitful database for the further development of the semi-industrial FDCA derivatives production process. Three Mn/Ni cation ratios of $LaMnO_{3-d}$, $LaMn_{0.5}Ni_{0.5}O_{3-d}$, and $LaNiO_{3-d}$ catalysts were selected and prepared by the Sol-Gel method. The bulk chemical species and oxidation states of secondary metal elements (Mn and Ni) for all synthesized perovskite-oxide catalysts were characterized by X-ray absorption near edge structure (XANES). The result of the distinct ratio of Mn^{3+}/Mn^{4+} ions significantly affected the oxidation reaction of HMF. The $LaMn_{0.5}Ni_{0.5}O_{3-d}$ and $LaMnO_{3-d}$ catalysts achieved high catalytic performance for the HMF oxidation reaction at 120 °C for 4 hrs. The kinetic parameters and activation energy were successfully estimated and reported.

1. Introduction

Nowadays, the number of plastic uses has drastically increased for various applications. Most plastics contain hazardous chemicals that are difficult to degrade. Consequently, plastic garbage can linger in the ecosystem for up to 450 years. Moreover, decomposing every plastic garbage by burning releases harmful gases like dioxins, furans, carbon monoxide, etc. - causing serious air pollution problems. To overcome these demerits, researchers have been developing biodegradable plastics derived from agricultural wastes. One of novel biorefinery derivatives is 2,5-furan dicarboxylic acid (FDCA) - a substrate converted from sugar-based chemicals, i.e., glucose, fructose - used as a raw starter to produce polyethylene 2,5-furan dicarboxylate (PEF). The FDCA molecule is typically derived by the oxidation of hydroxymethylfurfural (HMF), also known as 5-hydroxymethylfurfural (5-HMF). Many researchers have described a mechanism pathway of the 5-HMFoxidation reaction as shown in Figure 1 (Dutta and Bhat 2022).

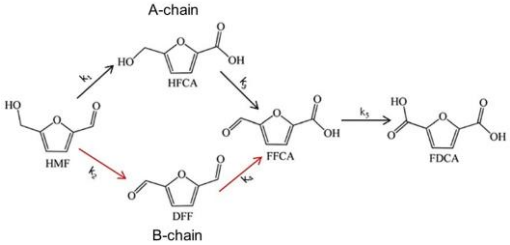

Figure 1: General purposed pathway of HMF oxidation (Dutta and Bhat 2022).

Paper Received: 25 January 2023; Revised: 9 April 2023; Accepted: 23 June 2023
Please cite this article as: Wattanachai P., Soisuwan S., Boonruam P., Panpranot J., Kidkhunthod P., Upasen S., 2023, Kinetics of Catalytic Oxidation of Hydroxymethylfurfural to 2,5-Furandicarboxylic Acid over $LaMn_{1-x}Ni_xO_{3-d}$ Perovskite Oxide, Chemical Engineering Transactions, 105, 319-324 DOI:10.3303/CET23105054

The reaction path followed in the A-chain reaction starts with an oxygen molecule attached to the aldehyde group of HMF forming a carboxyl group. The first intermediate substrate was produced, called 5-Hydroxymethyl-2-furancarboxylic acid (HMFCA). One mole of oxygen further reacts to the arm of the HMFCA hydroxyl group converting to an aldehyde group, producing the second intermediate called a 5-formylfurancarboxylic acid (FFCA). In the end, the aldehyde group of FFCA reacted with an oxygen molecule becoming a 2,5-furandicarboxylic acid product (FDCA). In the B chain, another intermediate intermediate named 2,5-diformylfuran (DFF) was produced by oxygen attached to the hydroxyl group of HMF to break down into an aldehyde group. Then, the DFF reacts further with oxygen to form FFCA and FDCA, consecutively. According to various studies, the most popular catalysts for the oxidation of HMF due to its outstanding catalytic stability are noble metals on different supports. The noble metal catalysts resulted in high synthesis efficiency and FDCA yield as high as 98-99%, but the high-cost metal is not accepted commercially. By dint of this drawback, solid metal oxides in different structures such as perovskite oxide have been found of great interest in catalytic applications. In a previous work (Soisuwan, Boonruam, et al. 2022), $LaMn_xNi_{1-x}O_{3-d}$ perovskite oxide catalyst demonstrated a great performance on HMF oxidation. It was due to the high relative O^{2-}_{latt}/O_{ads} ratio which is affected by the distinct Mn/Ni ratio of the catalyst. However, a kinetic reaction analysis with an estimation of the reaction rate constant using this metal oxide catalyst should be well understood. Researchers mentioned that many factors affect the speed of a chemical reaction and insight into reaction mechanisms. For example, Alexander and co-workers (Gonzalez-Casamachin, Rivera De la Rosa et al. 2020) have found the estimated reaction rate constants for the oxidation of HMF using ZnO and polypyrrole (ZnO/PPy). The primary intermediate in the first oxidation was the HMFCA intermediate. Moreover, the oxidation reaction on the hydroxyl group of the HMFCA was more predominant than on the carbonyl group of DFF converting into an FFCA molecule. The FFCA transformed to FDCA in the last oxidation step has fast occurred since the reaction rate constant was higher than among other steps.

In this present study, the objective was to analyze the kinetic rate constant of HMF oxidation using perovskite oxide $LaMn_{1-x}Ni_xO_{3-d}$ following the purposed mechanism pathway (Figure 1). The temperature dependency of a reaction according to Arrhenius' law was also estimated. A comparison of catalytic efficiency between single- and double-perovskite oxide catalysts was made. The surface oxidation state properties of metals and oxygen moieties for the selected catalysts were analyzed by XANES techniques. Furthermore, the relationship between the kinetic reaction result, catalytic efficiency, and catalyst properties was also discussed.

2. Materials and Methodology

2.1 Chemicals and Catalyst Synthesis

The AR grade of 98% purity of $La(NO_3)_3.6H_2O$, $Mn(NO_3)_2.4H_2O$, and $Ni(NO_3)_2.6H_2O$ purchased from KEMAUS and Ajex Finechem company were used in this research. The 99% purity of Hydroxymethyl furfural (HMF) and all suspected products described in the previous section were purchased from Sigma-Aldrich. Pure nitrogen gas (99.95%) for oxidation was supplied by Linde (Thailand) PCL. All chemicals were used as received without further purification or treatment.The $LaMnO_{3-d}$ (LMO), $LaNiO_{3-d}$ (LNO), and $LaMn_{0.5}Ni_{0.5}O_{3-d}$ (LMNO) perovskite oxide were synthesized by the Sol-Gel method, described in previous work (Soisuwan, Boonruam et al. 2022). Briefly, 0.1 M lanthanum nitrate solution (8.66 g $La(NO_3)_3.6H_2O$) was prepared in 200 mL DI water. The $Mn(NO_3)_2.4H_2O$ and ($Ni(NO_3)_2.6H_2O$) precursors were added into the lanthanum nitrate solution by the molar ratio of La:Mn: Ni equal to 1:0:1, 1:0.5:0.5 and 1:1:0. While the mixed solution kept stirring for several minutes, an amount of 8.4 g citric acid (molar ratio of total metal to citric acid equals to 1:1) was slowly added. [Note: This study used citric acid as a metal binder to form a metal citrate complex solution.] The pH solution of 6-7 was adjusted by adding 10 vol.% ammonia solution ($NH_3.H_2O$). It was dropped as slowly as possible to prevent the formation of metal hydroxide precipitates. The mixed solution was kept at 80 °C under vigorous stirring for 24 hrs. After the solution became completely gelatin appearance, the gelatin was then evaporated at 105 °C for 6 hrs. Finally, the dried powder precursor was calcined at 800 °C under atmospheric pressure for 12 hrs.

2.2 HMF Oxidation Experiment

The HMF oxidation reaction experiment was carried out in a batch reactor using a 100 mL Teflon cylinder reactor which was placed inside a high-pressure autoclave equipped with a temperature and pressure controller. According to the previous work (Soisuwan, Boonruam, et al. 2022), the reaction conditions were tested with one mmol of HMF, nine mmol of tert-butyl hydroperoxide (TBHP), and 0.01 g/mL of catalyst loading. A 0.1 M HMF solution was prepared in 20 mL pure acetonitrile solvent. Additionally, 0.261 mmol Na_2CO_3 was added to the mixed solution. [Note: The pH value of the solution was measured both before and after each reaction run.] The well-mixed solution in the Teflon cylinder was placed inside the autoclave equipment. Then, it was pressurized in 5 bar N_2 gas and kept heating at temperatures 80 - 120 °C with a stirring speed of 300 rpm. To explore the

rate of reaction, experiments were carried out in five different reaction times from 15 - 240 mins. In the end, the solid catalyst was separated from the liquid sample. The collected liquid sample was analyzed by HPLC techniques to quantify all products (DFF, HMFCA, FFCA, and FDCA) including the remaining HMF reactant.

2.3 Characterization

The structure of the LMNO, LMO, and LNO catalysts was investigated by the XANES technique at beamline BL 5.2 of the Siam Photon Laboratory, Synchrotron Light Research Institute (SLRI), Thailand. The beamline energy range and beam size are 1.25 - 12.1 keV and 10 x 1 mm^2. The XANES experiment was operated under the absorption mode for both the Ni K-edge and the Mn K-edge. [note: the La element could not be examined due to unavailable data and technical problems] The XANES spectra were collected using a beam current of 126.88 - 145.56 mA and 1.1 - 1.7x10^{11} photon.s^{-1}. The Ni and Mn XANES spectra were processed and analyzed after data background subtraction in the pre-edge and post-edge regions by using ATHENA software. Quantitative characterization of all substrates in the liquid samples from the HMF oxidation reaction was analyzed by high-performance liquid chromatography (HPLC) using Agilent Infinity II models. A photodiode array (PDA) detector was used at a wavelength of 260 and 280 nm. The stationary column was a Cosmosil 5C18-AR-II with a size of 250 x 4.6 mm. The mobile phase solution was pure acetonitrile and 50 mM ammonium acetate buffer solution. A pH of 5.2 of the buffer solution was adjusted using acetic acid. The conversion and selectivity of each investigated component were calculated as described elsewhere (Soisuwan, Boonruam et al. 2022).

3. Result and discussion

3.1 Mn/Ni oxidation states and its effect

The percentage of analyzed compounds and oxidation state of the bulk Mn and Ni metals characterized by the XANES technique were estimated (Upasen, Sarunchot, et al. 2022) and summarized in Table 1. The average Ni and Mn oxidation states for double perovskite oxide were higher than those for single perovskite oxide. This observation is compliant with the work by Alkhalifah and co-workers (Alkhalifah, Howchen, et al. 2022), in which the effective Ni oxidation state changes when incorporating the Mn species into the hosted LNO crystal. Hence, the difference in Ni and Mn oxidation states for all prepared catalysts might result in a different number of lattice/surface oxygen to compensate for the chemical oxidation state in the crystal solid. This chemical characteristic might affect the performance of the HMF oxidation reaction.

Table 1: The summary of bulk chemistry analysis for all investigated samples.

Sample	Abbr.	Metal ions percent (%)					Abs. edge position (eV)		Avg. OS.	
		Ni	Ni^{2+}	Mn^{4+}	Mn^{3+}	$Mn^{2.67+}$	Ni	Mn	Ni	Mn
$LaMnO_{3-d}$	LMO	n/a	n/a	52.7	47.3	n/a	n/a	6553.2	n/a	3.5
$LaNiO_{3-d}$	LNO	18.6	81.4	n/a	n/a	n/a	8348.3	n/a	1.6	n/a
$LaMn_{0.5}Ni_{0.5}O_{3-d}$	LMNO	2.3	97.7	83.3	3.2	13.5	8349.9	6554.1	1.9	3.8

Note: n/a was not applicable. OS. stands for oxidation state.

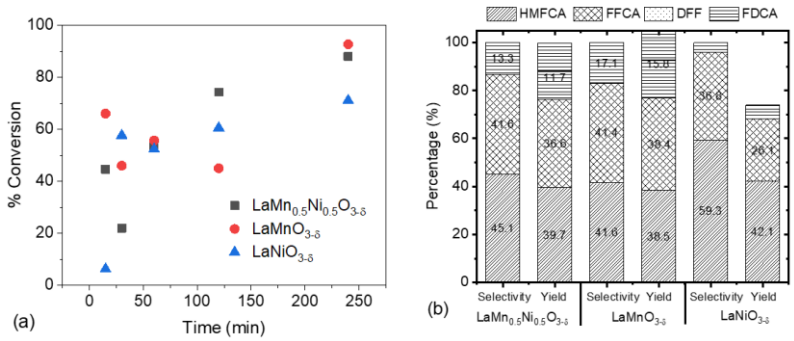

Figure 2: Single- and double perovskite oxide catalyst effect on catalytic oxidation reaction: (a) HMF conversion (b) yield and selectivity.

The effect of the Mn/Ni ratio on the HMF oxidation activity is illustrated in Figure 2a. For 4 hrs reaction time, the highest percentage of HMF conversion showed 71.1%, 88%, and 92.7%, for using LNO, LMO, and LMNO catalyst, respectively. The formation of HMFCA and FFCA intermediates through the HMF oxidation process for all catalysts was highly favorable (Figure 2b). The DFF intermediate was not detected in this research. Only

15.8% and 11.7% FDCA yield for using the LMO and LMNO catalysts, respectively, were detected. Giannakoudakis and co-workers (Giannakoudakis, Nair, et al. 2019) found that various Mn oxidation states also caused a limitation of oxidative capability toward the HMF. Both single perovskite-oxide and double perovskite-oxide with Mn ion coordinate in oxygen octahedral achieved high catalytic performance for the HMF oxidation reaction. Furthermore, it was related to the bulk Mn^{4+} characteristic of all catalysts as discussed earlier. The LMNO sample presented in a large proportion of Mn^{4+} might cause an excess of oxygen in the crystal structure. In general, the more oxygen species on the surface catalyst exist, the greater the decay in the proton of the HMF molecule (Giannakoudakis, Nair et al. 2019). The reduction of the proton allows water to form more easily. In the case of insufficient surface oxygen, the formation of water molecules was difficult because HMF requires high energy to cleavage C-C bonds up to 350 kJ/mol for conversion to HMFCA. As a result, activity decreased as revealed by the gradual decrease of conversion as the reaction continued.

3.2 Temperature, kinetic parameters, and activation energy

Figure 3 shows the HMF oxidation activity and selectivity using LMNO catalyst at various temperatures. The HMF conversion was inclined as an increment of reaction time (Figure 3a). The oxidation catalytic activity using LMNO catalyst was highly sensitive to increased temperature. This was consistent with the thermodynamic analysis of HMF oxidation described in the literature (Gao, Yin et al. 2018). The selectivity and production yield (Figure 3b) were also strongly influenced by the temperature. The highest FDCA selectivity and yield of 13.3% and 11.7%, respectively, were detected at 120 °C. The HMFCA and FFCA intermediates were also highly converted into FDCA with an increase in temperature. However, it should be noted that undesirable reactions with high temperatures, for example, a formation of open ring products such as levulinic and formic acid, are concerned and reported in the literature (Gonzalez-Casamachin, Rivera De la Rosa et al. 2020).

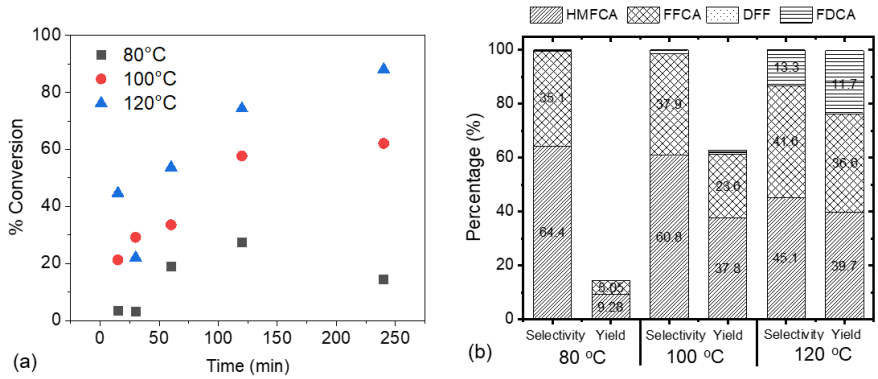

Figure 3: Temperature effect on HMF oxidation reaction using LMNO catalyst: (a) HMF conversion (b) yield and selectivity.

Since the DFF was not observed in this study, the rate constant of k_2 and k_4 are assumed to be null. The pathway of the HMF oxidation step occurring in the A-chain (Figure 1) was proposed. The reaction rate equation with the common presumption of a first-order reaction for each step can be written:

$$\frac{d[HMF]}{dt} = -(k_1+k_2)[HMF] \quad (1)$$

$$\frac{d[HMFCA]}{dt} = k_1[HMF] - k_3[HMFCA] \quad (2)$$

$$\frac{d[FFCA]}{dt} = k_3[HMFCA] - k_5[FFCA] \quad (3)$$

$$\frac{d[FDCA]}{dt} = k_5[FFCA] \quad (4)$$

The differential forms for the change in concentrations of HMF, HMFCA, FFCA, and FDCA can be manipulated. Hence, the integration expression for each reaction rate can be derived in a function of time-dependent concentration as following equations:

$$\ln[HMF] = -k_1 t + \ln[HMF]_0 \quad (5)$$

$$\ln[HMFCA] = (-k_1 + k_3)t \quad (6)$$

$$\ln [FFCA] = (-k_1-k_3)\, t + (\ln K_1 + \ln K_3) \quad (7)$$

To estimate each k value, Figure 4 (a) plots experimental concentration data versus time (Eq. 5-7), where $K_1 = \frac{k_1 k_3 [HMF]_0}{(k_3-k_1)(k_5-k_1)}$ and $K_2 = \frac{k_1 k_3 [HMF]_0}{(k_3-k_1)(k_5-k_3)}$. The rate constants (k value) solved from the proposed mathematical models (Eq. 5-7) are summarized in Table 2. For all catalysts, the estimated rate constants of the three sequential steps occurring in the A-chain (Figure 1) resulted in the order of $k_1 > k_3 > k_5$. According to the literature (Zuo, Chaudhari et al. 2016), the oxidation step of FFCA converting into FDCA was a rate-limiting step. It means that the oxidation of FFCA was the slowest step among others. For step FFCA to FDCA, the carboxyl group causes the electrons of the furan ring to be attracted toward itself, making them less available to stabilize the free radical. The fastest reaction step was from HMF to HMFCA, indicating the higher reactive on aldehyde than carboxyl and hydroxyl groups.

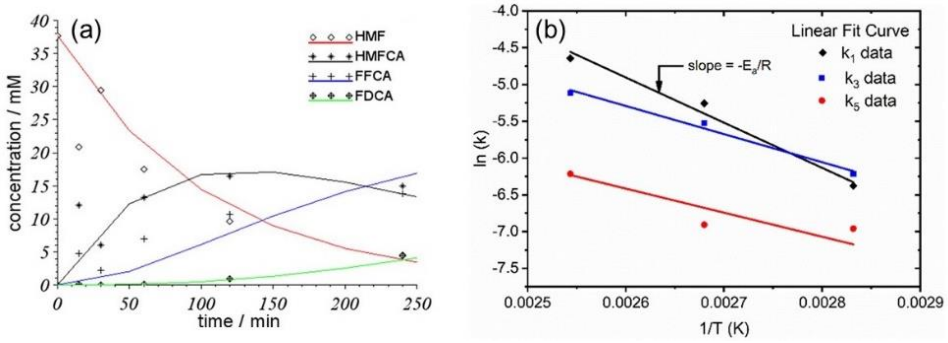

Figure 4: (a) Mathematical fitted model of concentration vs. time, (b) temperature dependency of HMF oxidation.

Table 2: The kinetic parameters and activation energy for various steps.

Catalyst	T (°C)	Rate Constant (L^2/mol.g.sec)			E_a (kJ/mol)				k^0 (L^2/mol.g.s)			
		k_1	k_3	k_5	1	2	3	4	1	2	3	4
LMO	120	0.010	0.008	0.003	-	-	-	-	-	-	-	-
LNO	120	0.006	0.004	0.003	-	-	-	-	-	-	-	-
	80	0.002	0.002	0.001								
LMNO	100	0.005	0.004	0.001	51.1	n/a	31.8	27.2		64729.4	105.6	8.2
	120	0.010	0.006	0.002								

Note: k_2 and k_4 were the reaction rate constant of DFF intermediate occurring in the B-chain.

According the Arrhenius's equation, three temperature point data of each reaction rate (k_1, k_3, and k_5) for the LMNO catalyst was well fitted by using the Linear regression model, shown in Figure 4 (b). The estimated E_a values (Table 2) corresponded to the typical E_a range for the reaction in the solution phase. Generally, the E_a values for chemical reactions in the solution phase are 8.3–150.7 kJ/mol (Gonzalez-Casamachin, Rivera De la Rosa et al. 2020). The mechanism to obtain HMFCA was irreversible, where activation E_{a1} was 51.1 kJ/mol (Table 2) - the reaction rate susceptible to temperature-dependent effect was preferred. It implies that the HMF oxidation was being attacked by •OH species generated on the surface of the LMNO catalyst. Contrary to other observations (Gonzalez-Casamachin, Rivera De la Rosa et al. 2020), the initial step of HMF oxidation was more predominant in the molecules/radicals transportation mechanism. The activation energy E_{a3} and E_{a4} were 31.8 and 27.2 kJ/mol (Table 2), respectively, indicating that a transport mechanism was more predominant than a completely reactive mechanism. However, the selectivity of FFCA and FDCA was increased when increasing the temperature (see Figure 4a). This result indicates a contrary to the prediction of the reaction mechanism - the oxidation of the carbonyl functional group on HMFCA and FFCA was susceptible to increment in temperature.

4. **Conclusion**

The $LaMn_{0.5}Ni_{0.5}O_{3-d}$, $LaMnO_{3-d}$, and $LaNiO_{3-d}$ catalysts were successfully synthesized by the Sol-gel method. These three catalysts were quantified for Mn and Ni metals by the XANES technique. The LMNO and LMO which present the Mn^{4+} content and are related to the excess oxygen in the crystal structure significantly affect the reactivity of HMF oxidation. The percentage of FDCA yield revealed 15.8% and 11.7% for LMO and LMNO catalysts, respectively. The selectivity of FFCA and FDCA depended upon temperature. The kinetic parameters were successfully estimated and predicted the fastest transformation from HMF to HMFCA intermediate. The activation energy via the first step of HMF oxidation for the LMNO catalyst predicted the susceptibility of reaction rate to temperature-dependent effect.

Nomenclatures

[HMF] – HMF concentration, molar
[HMFCA] – HMFCA concentration, molar
[FFCA] – FFCA concentration, molar
[DFF] – DFF concentration, molar
[FDCA] – FDCA concentration, molar
E_a – Activation energy, kJ/mol
k^0 – Pre-exponential factor, L^2/mol.g.s
R – Molar gas constant, 8.314 $J.K^{-1}.mol^{-1}$
T – Reaction temperature, K
t – Reaction time, second
k_1-k_5 – Reaction rate for steps 1-5, L^2/mol.g.sec

Acknowledgments

Burapha University and Thailand Science Research and Innovation *(*TSRI*) (*Grant No. 43.2/2566*)* and Research Team Promotion Grant financially supported this work. In addition, the authors are grateful for the acknowledgment of Ms. Kittima Kroekritvanich and Ms. Nattanit Benjangvisanu. This project was under the Research Unit of Developing Technology and Innovation of Alternative Energy for Industries, Chemical Engineering, Burapha University, and collaborated with the CAT-REAC industrial project, Chulalongkorn University.

References

Alkhalifah M. A., Howchen B., Staddon J., Celorrio V., Tiwari D., Fermin D. J., 2022. Correlating Orbital Composition and Activity of LaMnxNi1−xO3 Nanostructures toward Oxygen Electrocatalysis. Journal of the American Chemical Society 144(10), 4439-4447. http://dx.doi.org/10.1021/jacs.1c11757

Dutta S., Bhat N. S., 2022. Chemocatalytic value addition of glucose without carbon–carbon bond cleavage/formation reactions: an overview. RSC Advances 12(8), 4891-4912. http://dx.doi.org/10.1039/D1RA09196D

Gao T., Yin Y., Fang W., Cao Q., 2018. Highly dispersed ruthenium nanoparticles on hydroxyapatite as selective and reusable catalyst for aerobic oxidation of 5-hydroxymethylfurfural to 2,5-furandicarboxylic acid under base-free conditions. Molecular Catalysis 450, 55-64. http://dx.doi.org/10.1016/j.mcat.2018.03.006

Giannakoudakis D. A., Nair V., Khan A., Deliyanni E. A., Colmenares J. C., Triantafyllidis K. S., 2019. Additive-free photo-assisted selective partial oxidation at ambient conditions of 5-hydroxymethylfurfural by manganese (IV) oxide nanorods. Applied Catalysis B: Environmental 256, 117803. http://dx.doi.org/https://doi.org/10.1016/j.apcatb.2019.117803

Gonzalez-Casamachin D. A., Rivera De la Rosa J., Lucio–Ortiz C. J., Sandoval-Rangel L., García C. D., 2020. Partial oxidation of 5-hydroxymethylfurfural to 2,5-furandicarboxylic acid using O2 and a photocatalyst of a composite of ZnO/PPy under visible-light: Electrochemical characterization and kinetic analysis. Chemical Engineering Journal 393, 124699. http://dx.doi.org/https://doi.org/10.1016/j.cej.2020.124699.

Soisuwan S., Boonruam P., Wattanachai P., Morillas H., Panpranot J., Praserthdam P., Upasen S., 2022. Capability of single and double elements doped perovskite oxide catalysts in 5-hydroxymethyl furfural oxidation. Biomass Conversion and Biorefinery online published: 23 December 2022. http://dx.doi.org/10.1007/s13399-022-03673-w.

Upasen S., Sarunchot G., Srira-ngam N., Poo-arporn Y., Wattanachai P., Praserthdam P., Ngaotrakanwiwat P., Panpranot J., Soisuwan S., 2022. What if zeolite LTA4A and zeolite LTA5A used as Nickel catalyst supports for recycling carbon dioxide to green fuel methane. Journal of CO2 Utilization 55: 101803.

Zuo X., Chaudhari A., Snavely W., Niu F., Zhu H., Martin K., Subramaniam B., 2016. Kinetics of Homogeneous 5-Hydroxymethylfurfural Oxidation to 2,5-Furandicarboxylic Acid with Co/Mn/Br Catalyst. AIChE Journal 63, 162-171. http://dx.doi.org/10.1002/aic.15497